Proceedings of the International Conference on Heat Exchanger Fouling and Cleaning - 2024 (Peer-reviewed)
April 21–26, 2024, Lisbon, Portugal; Editors: H.U. Zettler and E.M. Ishiyama

# EXPERIMENTAL AND NUMERICAL INVESTIGATIONS OF CLEANING BASED ON FUNDAMENTAL MODELLING OF MASS TRANSFER

***K.P. Deshmukh[1], R.S. Cant[2], D. Arlov[3] and D.I. Wilson[1]**
[1] Department of Chemical Engineering and Biotechnology, Philippa Fawcett Drive, Cambridge, CB3 0AS, UK (kd391@cam.ac.uk)
[2] Department of Engineering, Trumpington Street, Cambridge, CB2 1PZ, UK
[3] Tetra Pak Processing Systems AB, Research & Technology, Ruben Rausings Gata, 221 86 Lund, Sweden

## ABSTRACT

The removal of a model food soil, a soluble coffee extract, from stainless steel plates by the passage of cold water has been investigated for two geometries: in a radial flow cell, where the flow is laminar and steady (but not simple), and in a rectangular duct where the flow is turbulent and fully developed. The rate of removal is assumed to be controlled by diffusion in the liquid phase, *i.e.* convective mass transfer where the liquid is moving. The experimental cleaning data, based on the local time to clean, are compared with detailed numerical models, where CFD simulations provide the velocity field for the mass transport equation. The diffusion coefficient for the coffee soil is determined separately by two different methods. The radial flow cell exhibits two cleaning fronts, related to the presence of recirculation zones, while cleaning in the duct features striations associated with periodic turbulence patterns. The results indicate that modelling even the simplest removal mechanism is not straightforward.

## INTRODUCTION

A fouled surface will normally need to be cleaned, incurring penalties in terms of lost productivity; energy, chemicals and solvent consumption; and the disposal of wastes generated [1, 2]. These all impact the financial, environmental and sustainability performance of the operation. In sectors such as the food and pharmaceutical sector, cleaning-in-place (CIP) operations are conducted regularly by circulating cleaning solutions through the unit. Optimising these operations requires reliable understanding of the impact of equipment geometry, fouling phenomena and cleaning mechanisms, preferably expressed in terms of quantitative models [3].

Fouling deposits are, however, rarely simple and this leads to complex cleaning mechanisms, which have been characterized in terms of chemical nature (*e.g.* [4]) and, more recently, in terms of physical and chemical interactions ([3, 5, 6]). This complexity has prompted the use of 'model' deposit or soil layers in order to establish the factors determining cleaning behaviour and removal rates (see [7] for a review of model food soils). In this context a 'model' soil or deposit is one whose behaviour is understood and reproducible, so that results obtained in testing these systems are free from ambiguity in interpreting the mechanism involved, and subject to low experimental variability. These experimental studies yield estimates of cleaning rates (in effect, removal fluxes) as a function of local parameters such as temperature, shear stress imposed on the soil-cleaning fluid interface, and heat or mass transfer rates. In an ideal experiment these parameters will be known, giving a cleaning law that can be used as a boundary condition in a flow simulation replicating the equipment (*e.g.* [8]). Modern computational fluid dynamics (CFD) codes are able to predict the flow patterns of Newtonian liquids in steady cases with reasonable accuracy, and one may expect that they should be able to predict the associated cleaning behaviour, in the same way that heat transfer (in clean systems!) can be predicted.

There are some challenges in this approach. Firstly, fouling and cleaning is rarely uniform as manufacturing lines feature items with complex geometry and thus non-uniform flow patterns, spatially variable and often unsteady rates of momentum, mass and heat transfer. Whilst the tubesides on shell-and-tube and annular heat exchangers feature relatively simple flow patterns, the corresponding shellside flows, and those in tubular and plate heat exchangers, are not. A large number of experiments would need to be performed to carry the full range of conditions likely to arise in a unit in order to identify a compressive cleaning law. Secondly, in the food, pharmaceutical and bioprocessing sectors cleaning performance is assessed on the basis of removal of almost all deposited material, rather than restoration of process performance, so understanding how flow patterns give rise to low rates of cleaning is important.

In this work we have employed a model soil whose removal should be able to be predicted using fundamental principles rather than one that replicates how a real (complex) deposit behaves, in



ISBN: 978-0-9984188-3-4; Published online www.heatexchanger-fouling.com

order to establish the scope for CFD simulations to predict the removal rate in a non-simple flow. The soil is an initially smooth, even layer of instant coffee extract on stainless steel plates and is removed by the passage of cold water. The soil is soluble in the water and the removal rate is determined by mass transfer alone: the local rate is estimated by solving the convection-diffusion equation with velocity fields generated by CFD simulations.

Two geometries are considered: (*i*) a radial flow cell (RFC, Figure 1) with Reynolds numbers < 1000, where the flow is steady (but not simple) and (*ii*) a long rectangular duct (the slit flow cleaning cell, SFCC, Figure 2) at Reynolds numbers > 3000 where the flow is well understood and is not steady. An important feature is the absence of user-adjustable parameters: almost all inputs are either measured or estimated using separate experiments.

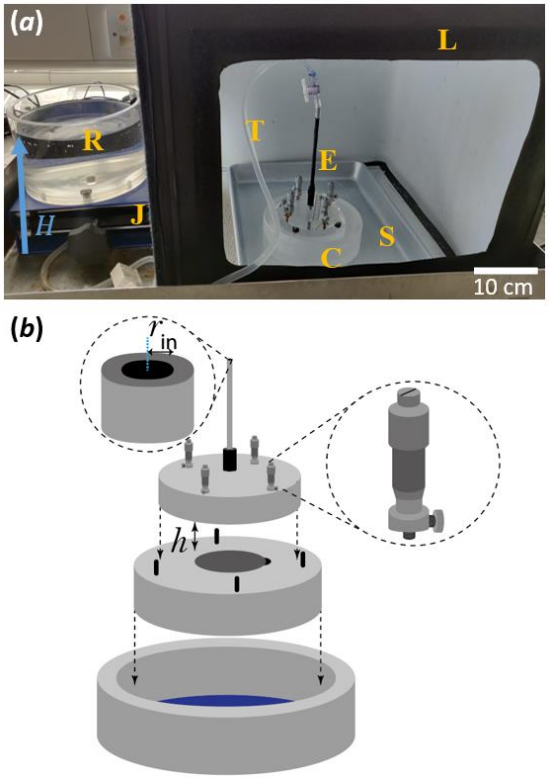


Figure 1. (*a*) photograph of the RFC and flow rig. C - radial flow cell; E - entry length; *H* - head of water providing pressure; J - lab jack, setting *H*; L – lightbox; R – reservoir; S - spill tray; T - tubing; (*b*) schematic showing key dimensions and micrometers setting gap height *h*.

## THEORETICAL

### Mechanism

The model deposit is soluble in water. Experiments indicated a saturation concentration, $C_{\mathrm{sat}}$, of 500 kg/m$^3$ at 20°C. The rate of removal is assumed to be determined solely by the rate at which dissolved soil diffuses into the flowing water, *i.e.* the deposit does not form a soft layer on contact with water which is set in motion by the shear force imposed on it by the flow (termed 'viscous shifting' in [5]). Similarly, fragments of soil (associated with 'cohesive breakdown'), or fragments along with patches of soil-free regions (associated with 'adhesive failure') were not observed. Evidence supporting this is provided by the SFCC experiments, where the surface immediately downstream of the test plates remains free of soil during experiments: no material is dragged downstream.

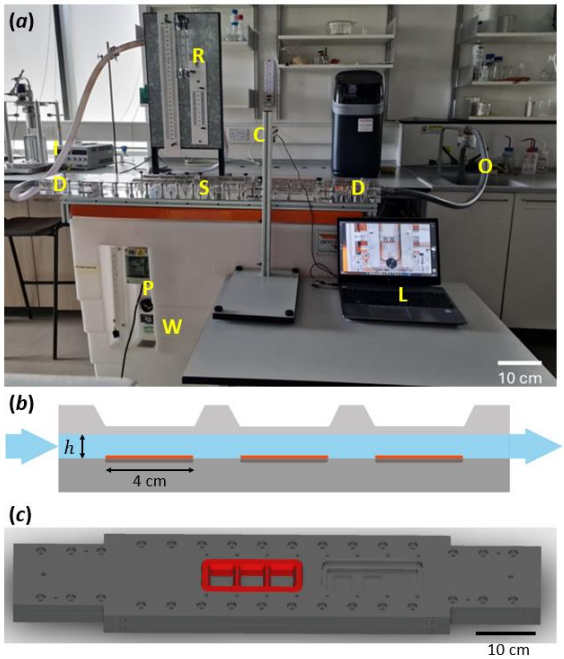


Figure 2. (*a*) Photograph of the SFCC rig. Labels: C – camera setup; D – diffuser; I – inlet pipe; L – laptop; O – outlet pipe; P – self-priming centrifugal pump; R – rotameter; S - slit flow cell; W - sump tank on Armfield flow bench; (*b*) schematic; (*c*) CAD model of the SFCC. One of the two detachable viewing panes is marked in red.

### Simulations

In the simulations, the deposit is modelled as a region of soluble wall, where the concentration of solute at the wall is $C_{\mathrm{sat}}$. Solute-free water ($C$ = 0) flows steadily into the duct at a specified flow rate and achieves a well-developed velocity profile upstream of the soil location. The local velocity field $\boldsymbol{u}$ is calculated by solving the Navier-Stokes equations in ANSYS Fluent 2019 R3 using the time-averaged k-$\omega$ turbulence model: the mesh, solution method and velocity fields for the RFC are discussed in Deshmukh *et al*. [9]: those for the SFCC will be reported in [10]. The concentration field is calculated by solving the steady state convection-diffusion equation in two dimensions, which in Cartesian coordinates ($x$, $y$) and vector notation are, respectively,



ISBN: 978-0-9984188-3-4; Published online www.heatexchanger-fouling.com

$$u\frac{\partial C}{\partial x} + v\frac{\partial C}{\partial y} = D\left\{\frac{\partial^2 C}{\partial x^2} + \frac{\partial^2 C}{\partial y^2}\right\} \quad (1a)$$

$$\boldsymbol{u}\cdot\nabla C = D\nabla^2 C \quad (1b)$$

where $u$ and $v$ are the components of $\boldsymbol{u}$ in the $x$ (downstream) and $y$ (normal to the surface) directions, respectively. Equation (1) is written in cylindrical coordinates for the RFC. Concentration $C$ is in mass units (the system is treated as dilute; the molecular identities are not known) and $D$ is the diffusion coefficient. The physical parameters; $D$, density and viscosity, are assumed to be independent of $C$. The local removal rate is calculated from the mass flux at the soluble wall, $N$, *viz*.

$$N = -D\left(\frac{\partial C}{\partial y}\right)_{y=0} \quad (2)$$

It should be noted that the duct dimensions do not change: the wall acts as source, with the mass flux determined by equation (2). In this respect the cleaning rate is described by a wall function, as employed by Joppa et al. [11].

The flux can be expressed in dimensionless form using the Sherwood number,

$$Sh = \frac{NL}{D(C_{\mathrm{sat}} - \bar{C}_{\mathrm{bulk}})} \quad (3)$$

where $L$ is a characteristic length (the duct height for both the RFC and the SFCC: in the tests reported here, 4 mm), $C_{\mathrm{sat}}$ is the saturation concentration (at the wall) and $\bar{C}_{\mathrm{bulk}}$ is the mixing cup bulk concentration. Analytical results exist for cases where $\bar{C}_{\mathrm{bulk}} \sim 0$ (*i.e.* slow mass transfer, $\bar{C}_{\mathrm{bulk}}$ does not change appreciably) and $N \approx k_{\mathrm{m}} C_{\mathrm{sat}}$, where $k_{\mathrm{m}}$is a film mass transfer coefficient which depends on spatial location and particularly distance downstream of the cleaning front (a mass transfer analogue of the Graetz problem in heat transfer).

Cleaning in these systems exhibits a cleaning front, caused by more rapid removal of soil upstream associated with boundary layer development. The local mass flux then depends on both location and time. Solving the associated Stefan problem is the subject of ongoing work and some preliminary results from this moving front problem are compared with experimental data here.

Calculating the mass flux requires a reliable estimate of the concentration gradient in the wall region. In simple terms the ratio of the thickness of the diffusion-controlled wall layer to the thickness of the momentum boundary layer is related to the Schmidt number, $Sc$ (for fully developed cases, to $Sc^{1/3}$)

$$Sc = \frac{\nu}{D} \quad (4)$$

where $\nu$ is the kinematic viscosity. For water at 20°C, $\nu \sim 10^{-6}$ m$^2$/s. For the coffee, $D$ is expected to be of order $10^{-10}$ m$^2$/s so $Sc$ ~ 10,000 and the diffusive length scale is very small: from Eq. [1], large gradients in $C$ can arise from modest velocities or small differences in convective rates. This simple analysis demonstrates that predicting mass transfer rates in solution for steady flows is a computationally challenging task: detailed calculation of time-dependent flows, *e.g.* where velocity fluctuations are captured [12], will require significant computational resource.

**Cleaning Model**

The removal of the soil layer is monitored visually, yielding the time taken to remove all visible soil at a particular location, $t_{\mathrm{c}}(r)$ or $t_{\mathrm{c}}(x,y)$. An average removal rate, in effect assuming zeroth order kinetics with rate constant $k'$, is estimated from

$$\delta = \delta_0 - k't \quad (5)$$

$$k' = \frac{\delta_0}{t_{\mathrm{c}}} = \frac{m_0}{\rho_{\mathrm{s}} N t_{\mathrm{c}}} \quad (6)$$

where $m_0$ is the initial soil coverage, $\delta_0$ the initial soil thickness and $\rho_{\mathrm{s}}$ its density, assuming it contains only solubles.

## EXPERIMENTAL

**Soil layers**

The test sections were prepared by coating layers of highly concentrated coffee solution using the spreading device reported by Cuckston [13] on circular (RFC; 50 mm diameter, 1 mm thick) or rectangular (SFCC; 50×40 mm, 2 mm thick) 316 stainless steel plates and allowed to dry at room temperature and humidity overnight. The solution was prepared by dissolving 50 g instant coffee in 100 mL deionised water at 21°C. Once cooled, it was centrifuged at 3,750 rpm for 300 s in order to separate out any solid components (*e.g.* fine powdered dispersants). Compositional analysis (Premier Analytical Services, UK) of the powder gave: carbohydrate, 39 wt%; fibre, 24.9 wt%; protein, 21.4 wt%; ash, 9.2 wt%; moisture, 5.3 wt%. Drying resulted in a mass loss of 70%. The thickness of the dried layers was measured using a scanning confocal thickness sensor (ConfocalDT IFS 2405-3, Micro-Epsilon, see [14]). In these tests, $\delta_0$ was 0.16 mm for the RFC and 0.18 mm for the SFCC.

**Diffusion coefficient**

The value of $D$ was determined using two methods: (*i*) magnetic resonance self-diffusion measurements, and (*ii*) spinning disc studies. In the former, coffee extract was dissolved in $D_2O$ at concentrations of 0.0015, 0.0625, 0.125 and 0.5 kg L$^{-1}$. 5 sets of peaks were evident, with a strong oligo- and polysaccharide peak evident at a chemical shift of ~ 3 ppm. Over the range of concentrations studied this species had an associated self-diffusion coefficient of $9.3\times10^{-11}$ m$^2$s$^{-1}$.



ISBN: 978-0-9984188-3-4; Published online www.heatexchanger-fouling.com

The second approach exploited the result that the convective mass flux from a spinning disc is uniform when the flow is in the laminar regime: an initially even layer should disappear at roughly the same time. The film mass transfer coefficient can then be estimated from

$$k_{\mathrm{m}} = \frac{\rho_{\mathrm{s}}\delta_0}{t_{\mathrm{c}}C_{\mathrm{sat}}} \qquad (8)$$

The analytical result for a spinning disc [15] gives

$$D = \left(\frac{\rho_{\mathrm{s}}\delta_0\nu^{1/6}}{0.62t_{\mathrm{c}}C_{\mathrm{sat}}\Omega^{1/2}}\right)^{3/2} \qquad (9)$$

where $\Omega$ is the angular velocity. Plots of $t_{\mathrm{c}}$ against $\Omega^{-1/2}$ should be linear, and yield an estimate of $D^{2/3}C_{\mathrm{sat}}$. A spinning disc apparatus [16] was repurposed to allow direct observation of samples: RFC sample plates were attached to the base of the plate, which was then lowered into a large glass bath of water and rotation started. A mirror allowed removal to be monitored and $t_{\mathrm{c}}$ identified. Linear plots of $t_{\mathrm{c}}$ against $\Omega^{-1/2}$ were obtained for $4 \leq \Omega \leq 44$ rad/s, giving $D^{2/3}C_{\mathrm{sat}}$. Separate experiments gave $\rho_{\mathrm{s}}$ = 1,350 kg m$^{-3}$ and $C_{\mathrm{sat}}$ = 500 kg m$^{-3}$, yielding $D = 1.1 \times 10^{-10}$ m$^2$s$^{-1}$. This was consistent with the self-diffusion results and a value of $1\times10^{-10}$ m$^2$s$^{-1}$ was used in the work presented here.

## RESULTS AND DISCUSSION

### Radial flow cell

The radial flow cell (Fig. 1) is described in detail in [9]: water flows through a 200 mm long inlet with radius $r_{\mathrm{in}}$ = 1 mm to give a steady, well developed flow into the gap between the plates. The base and top Perspex plates are larger than the test plate so the flow is steady at the edge of the test plate. The experiments reported here are for a single value of the aspect ratio, $AR \equiv h/r_{\mathrm{in}} = 4.2$. The cleaning parameter varied here is the Reynolds number, which by convention is the value for the flow in the inlet pipe.

Figure 3 shows a time series of cleaning in the radial flow cell. As time proceeds the darkness of the soil layer decreases and a circular clean region centred at the axis (obscured by the inlet tube), radius $a$, grows steadily outwards until it reaches an annular band which cleans noticeably more slowly. An annular clean region appears beyond the band, with outer radius $b$, which grows outwards steadily: the separating band eventually disappears. The latter often took longer than the experimental duration, such that $k'$ values were not always obtained.

The CFD simulations in Figure 4 elucidate this behaviour. The flow in the RFC is steady and laminar, and the change in direction at the inlet, combined with the expanding flow, combine to generate 3 recirculation zones (RZs) in the gap above the soiled plate. The location of the separating band coincides with the secondary RZ. Soil dissolved in this band will accumulate in the zone, thereby reducing the concentration driving force promoting dissolution, giving rise to slow removal rates: in effect, mass transfer from the RZ is limited by diffusion across the separatrix. By contrast, material dissolved in the primary RZ is advected over the top of the secondary zone, and mixes with solute added beyond the secondary zone. These results are consistent with previous studies of cleaning of systems with dead zones (*e.g.* [17]) but provide new insights as the 'dead zone' exists in a simple duct and upstream contributions affect cleaning rates.

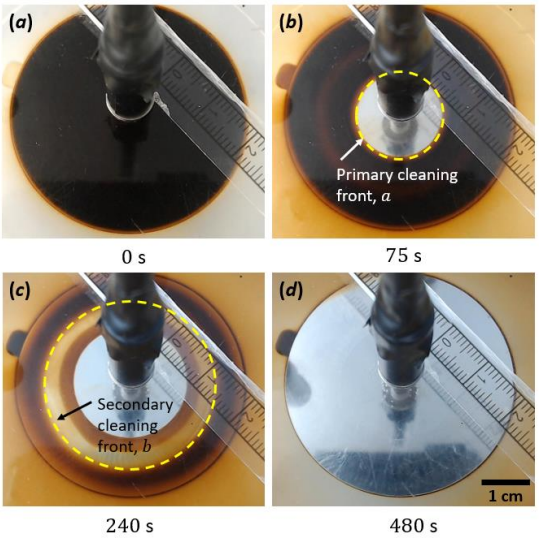


Figure 3. Images of cleaning in the RFC for $Re = 810$, $AR = 4.2$, at times indicated. (*a*) Start of the test; (*b*) Only primary cleaning front visible; (*c*) Secondary cleaning front visible; (*d*) Cleaned plate.

In these simulations, the liquid properties are assumed to be independent of soil concentration. Further complications could arise if the soil was very soluble and the properties of the liquid were strongly affected by concentration: a fully coupled simulation between mass and momentum transfer would be required to evaluate the impact of the recirculation zone.

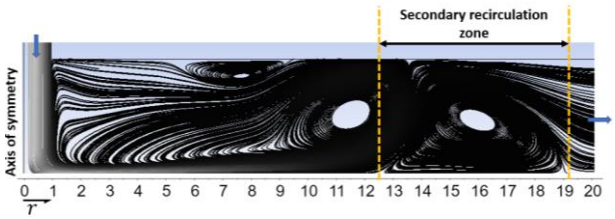


Figure 4. Streamline plot for RFC, with footprint of secondary recirculation zone marked. $Re = 810$, $AR = 4.2$, $h$ = 4 mm (same conditions as Fig. 3). Units of $r$ are dimensionless ($r_{\mathrm{in}}$ = 1 mm).

Figure 5(a) shows how the experimental cleaning rate, $k'$, varies with radial position $a$ (for the circular region) or $b$ (for the annular region). $k'$



ISBN: 978-0-9984188-3-4; Published online www.heatexchanger-fouling.com

decreases strongly with increasing $a$ and less strongly with $b$. The latter is almost an exponential decay: in this region the mean velocity $\propto r^{-1}$.

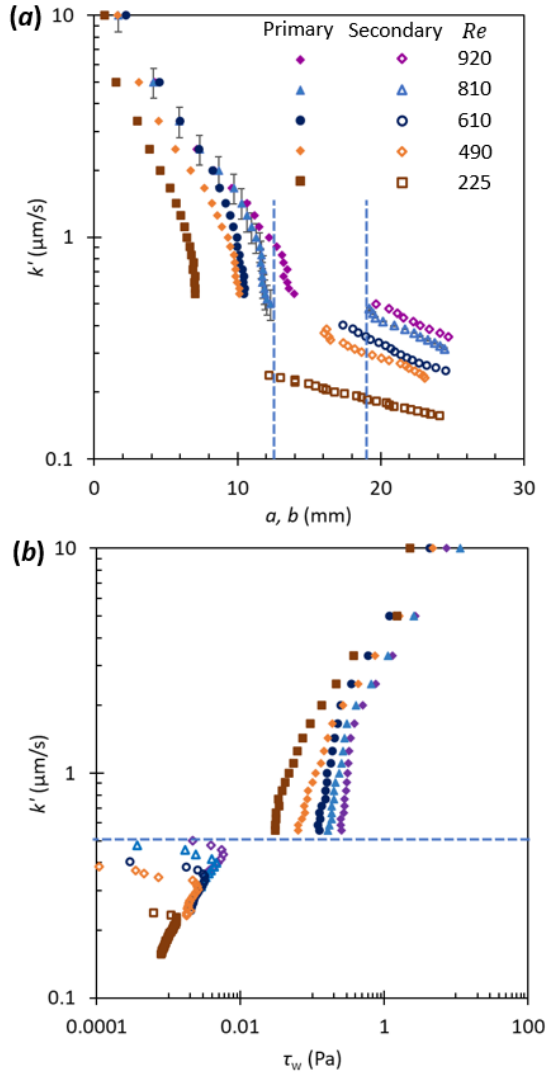


Figure 5. Variation of $k'$ in the RFC with ($a$) location, and ($b$) local wall shear stress. Solid symbols indicate primary cleaning front, open symbols secondary cleaning front. Vertical blue dashed lines in ($a$) indicate the location of the secondary RZ for $Re = 810$ indicated in Fig. 4. Horizontal dashed blue line in ($b$) indicates this transition, comparing the local wall shear stresses. Note log-linear axes in ($a$) and log-log axes in ($b$).

If cleaning was driven by mechanical action, the local cleaning rate would be expected to correlate strongly with local wall shear stress, $\tau_w$. The values of $\tau_w$ were extracted from the CFD calculations and the data are presented in this form in Fig. 5($b$). The cleaning rate is clearly not related to $\tau_w$ in a simple manner: upstream of the secondary RZ, the $k'$ values increase monotonically with $\tau_w$, but are dependent on $Re$ and exhibit an evident kink in the trend. The values for the secondary front follow a common trend, independent of $\tau_w$, for some, but not all, values.

Fig. 5(b) confirms that diffusive cleaning is not predicted by wall shear stress, and thus the need to identify the cleaning mechanism. Diffusion is a complex process to simulate owing to the coupling of the removal flux to the bulk concentration and hence driving force for cleaning, giving rise to the moving cleaning front. A soil subject to viscous removal whereby the material is eroded into the flow will not be subject to these complications.

Feeding the predicted flow pattern into eqns. (1-2) yields the concentration distribution and the local mass flux, which is plotted as $Sh$ in Fig. 6. The strong spatial variation arising from the presence of the secondary RZ is evident. High fluxes are predicted at $15 \leq r/r_{in} \leq 19$, yet these are not manifested in the cleaning results in Fig. 5: this may be because dissolved solute collects in the recirculation zone and this suppresses further dissolution in the vicinity of $r/r_{in} \sim 12.5$. Preliminary results from simulations show that there may be local thinning of the concentration boundary layer towards the foot of the secondary RZ (blue dashed line to the right) thereby causing an increase in $Sh$. Solute slowly diffuses out of the recirculation zone into the mainstream flow and this effectively determines the cleaning rate in the annular band. This is the subject of ongoing work.

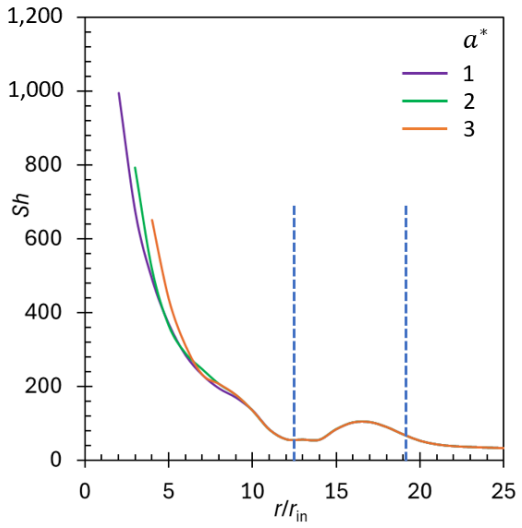


Figure 6. Effect of cleaning front location, $a$, on predicted dimensionless mass flux in the RFC for $AR$ = 4.2, $Re = 810$. Legend shows scaled values of $a$, *i.e.* $a^* = a/r_{in}$. Vertical blue dashed lines show the location of the secondary recirculation zone.

Figure 6 also shows the impact of the location of the cleaning front. There is no solute at $r < a$, so no flux is recorded for these values. When $r \sim a$ the flux is very large, with $Sh$ ~ 1,000: this value is determined by the resolution of the mesh. For $r/r_{in} \leq 10$ the local flux is very sensitive to where the cleaning front has reached: since this changes



ISBN: 978-0-9984188-3-4; Published online www.heatexchanger-fouling.com

with time, the rate at a given location changes (increases) with time. The moving front nature of cleaning driven by dissolution and diffusion is discussed later. There is no effect of the cleaning front downstream of the secondary RZ for the values of $a$ considered here.

Fig. 6 explains an important feature of Fig. 5, where the value of $k'$ at $r/r_{in}$ = 12.5 is very similar to that at $r/r_{in}$ = 19.2. In the experiments, the primary cleaning front stops growing just before the annular band appears. Fig. 6 shows that the flux at $r/r_{in}$ = 12.5 increases slightly as $a$ changes (*i.e.* with time) whereas that at 19 is constant, so the latter will take slightly longer to clean. This is consistent with the secondary cleaning front appearing just after the primary one comes to a stop. Inspection of Fig. 5(*b*) indicates that the wall shear stress at these two points differs by almost 2 orders of magnitude.

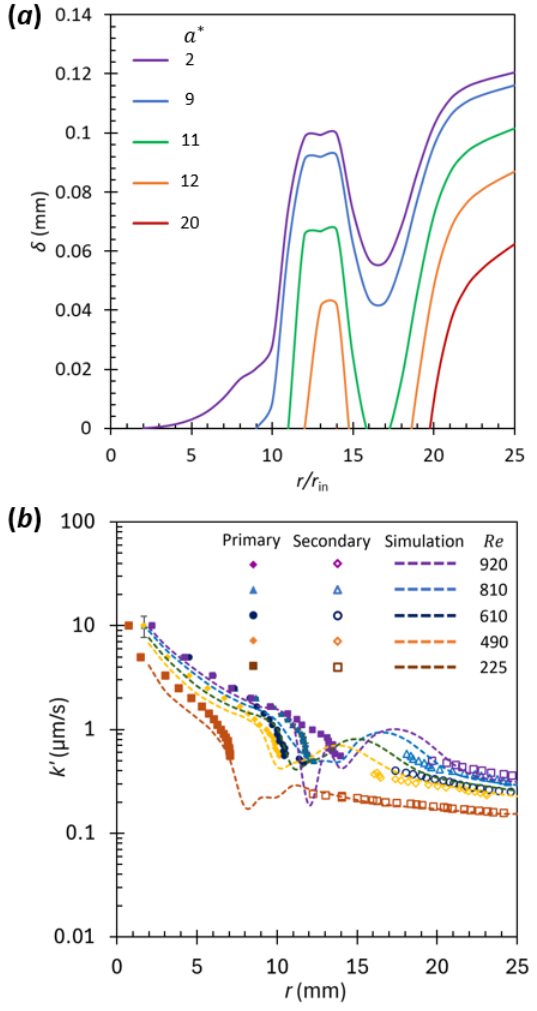


Figure 7. (*a*) Predicted soil thickness profiles in the RFC for $\delta_0$ = 0.16 mm, $AR$ = 4.2 at $Re$ = 810 for different positions of the (scaled) cleaning front location; (*b*) Comparison of measured and predicted $k'$ values.

The predicted mass flux results can be used to predict the instantaneous removal rate and thus the change in layer thickness. Figure 7(*a*) shows the predicted evolution for one case, which reflects the observed behaviour. The values of $k'$ were extracted and are presented along the experimental data in Fig. 7(*b*). There is a very good agreement between the experimental results and simulation predictions for the primary and secondary regions for all values of $Re$. The experimental results in the secondary recirculation zone are not shown due to the difficulty in tracking $a$; this is the subject of ongoing work.

**Slit flow cleaning cell**

The SFCC employs a rectangular flow section (height 4 mm, width 40 mm, approximately 1 m long) with test plates located sufficiently far downstream of the entrance to the rectangular duct that the flow is turbulent and well developed (confirmed by CFD simulations). The apparatus is constructed from polycarbonate. The schematic in Fig. 2(*b*) shows how the roof of the duct above the test plates is thin to allow good visual access. The time series of images in Fig. 8 shows three noteworthy features:

(*i*) Spanwise variation: removal is fastest in the central region, which is expected as the side walls exert drag on the liquid there, resulting in a non-uniform wall shear stress and hence velocity profile. In these experiments some soil was trapped under the side wall, resulting in material leaching into the bulk flow from the sides and slowing the rate of cleaning near the walls. This artefact was avoided in later tests by preparing soiled plates with the edges free of soil.

(*ii*) Striations in the soil: these patterns were reproducible, and the separation of cleaned bands that were non-dimensionalised by the duct height were found to be invariant with the Reynolds number. The soil layers are initially uniform, so the variations in local mass flux must arise from features in the flow. The existence of flow striations is well documented in the studies of turbulence [12, 18], and to our knowledge this is the first report of such features in cleaning studies. Visual confirmation was provided by dye injection (see Figure 9(a)). Striations have been observed in chemical reaction fouling deposition (*e.g.* [19], Figure 9(b)), demonstrating that fine scale features of turbulent flows can affect both deposition (fouling) and removal (cleaning). Given that the Reynolds number of the flows in the fouling and cleaning steps are unlikely to be similar (different chemical composition, temperature), the impacts are likely to differ between the two steps.



ISBN: 978-0-9984188-3-4; Published online www.heatexchanger-fouling.com

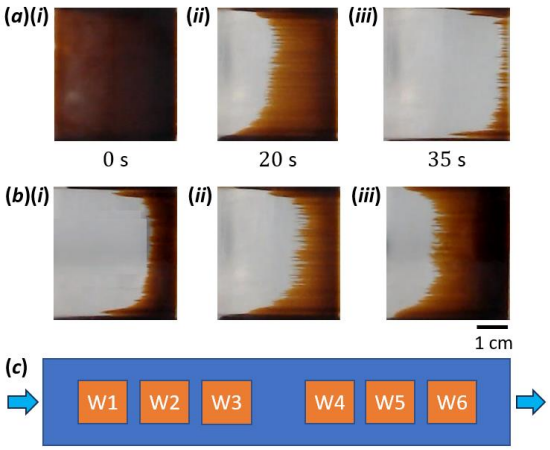


Figure 8. Cleaning in the SFCC: (*a*) time series at $Re$ = 7,500 at (*i*) 0 s, (*ii*) 20 s, (*iii*) 35 s for W5; (*b*) Window-by-window variation at 30 s from (*i*) W4 (*ii*) W5, (*iii*) W6; (*c*) schematic of window locations.

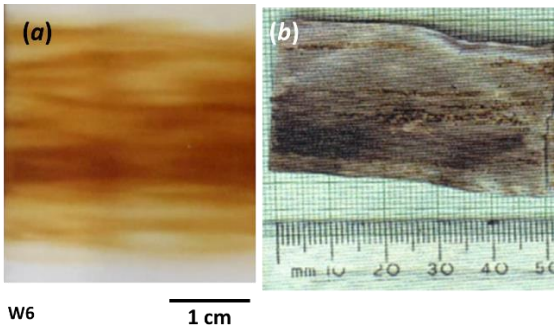


Figure 9. Striations in (*a*) dye visualization in SFCC at $Re$ = 3,800; (*b*) autoxidation reaction fouling deposits, flow inside tubes, $Re$ > 5,000 [19].

Strong local gradients arising from turbulence, termed 'turbulent bursts' [20], were the subject of much discussion in the fouling community in the 1980s. Some local mass fluxes will be larger than those calculated using averaged quantities; calculating these accurately would require very high-fidelity computation to deal with the highly dynamic velocity fields and short diffusion length scales. It appears that even the simplest removal mechanism (*i.e.* isothermal dissolution with little effect on liquid properties) can be challenging to predict: thought needs to be given to what level of agreement is acceptable.

(*iii*) Location: the upstream test section is consistently cleaned slightly faster than its neighbours, even though the bulk concentration does not change noticeably. This is consistent with a diffusion-driven removal process in which the concentration near the wall is progressively greater downstream. A mechanical removal mechanism, involving erosion, will be less sensitive.

**Quantifying removal**

Images such as those in Fig. 8 were analysed to determine the location of the cleaning front, yielding profiles such as those in Figure 10. The raggedness after 10 s is evidence of the striations. The material nearer the wall tends to be removed less quickly.

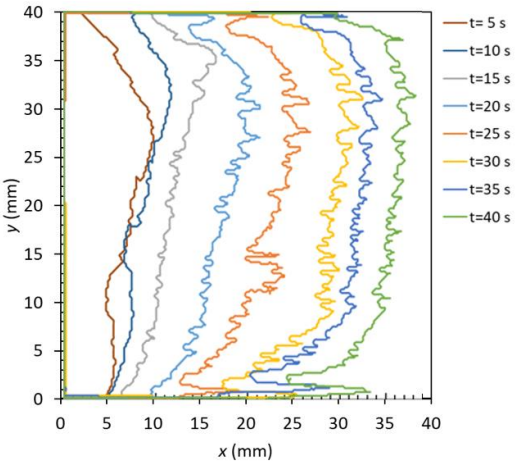


Figure 10. Evolution of SFCC cleaning front profile, $Re$ = 7,500, Figure 8(*a*).

Fig. 11 shows the computed dimensionless mass flux at the start of a test for a 2-D simulation. The variation is not as strong as in the RFC (Fig. 6) as the bulk velocity profile does not change noticeably with position: there are no recirculation zones (but secondary vortices are likely to arise in the corners).

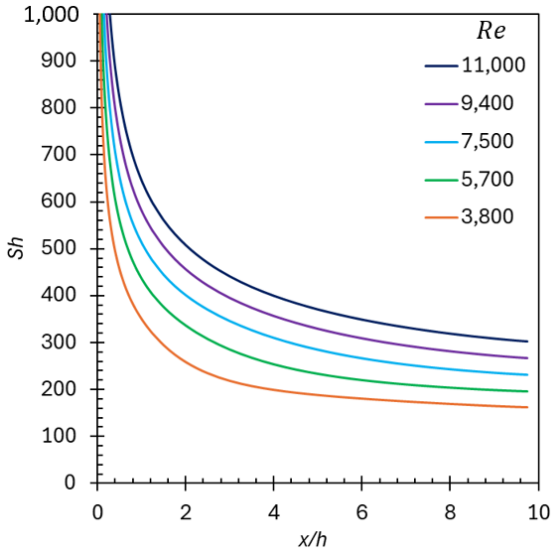


Figure 11. Effect of distance from the cleaning front, $x/h$, on dimensionless cleaning flux, 2-D simulation of SFCC.

Figure 12 shows the predicted evolution of soil layer thickness with time, denoted by the location of the cleaning front, $a$. The point where the layer thickness reaches zero allows $k'$ to calculated and the values are compared with the experimental ones in Figure 13. Better agreement is obtained between



ISBN: 978-0-9984188-3-4; Published online www.heatexchanger-fouling.com

the two data sets than for the RFC case except at the earliest time. Determining the mass transfer coefficient at low $x$ is the subject of ongoing work.

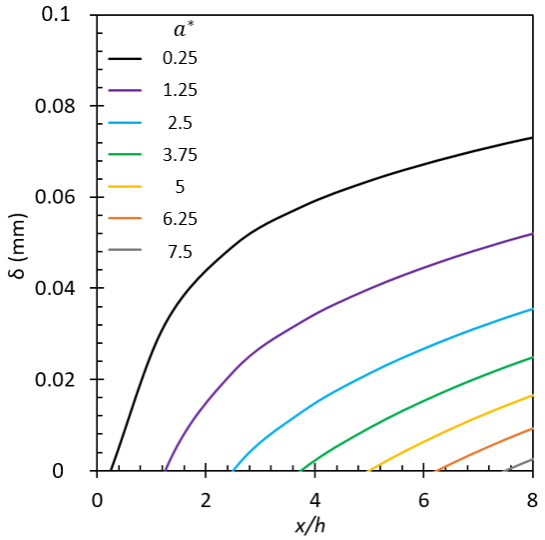


Figure 12. Soil thickness profiles at $Re = 7{,}500$ for different positions of the cleaning front. 2-D case.

It should be noted that the CFD in this case was based on time-averaged Reynolds stresses represented using the k-ω turbulence model, and was therefore unable to resolve transient features such as striations. The very good agreement in Figure 13 suggests that high resolution is not required to compute the final cleaning time for this application, unlike the RFC.

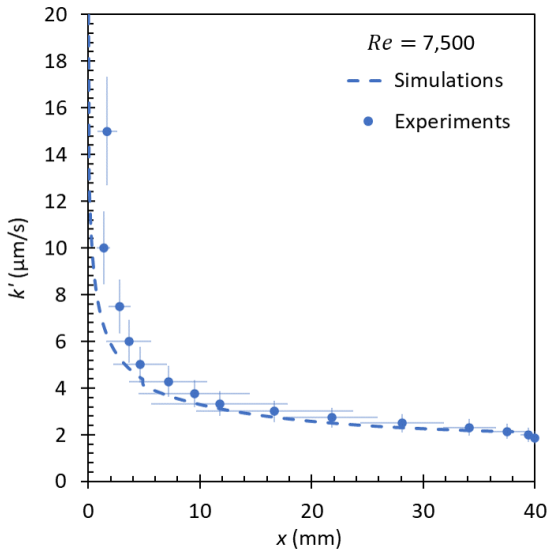


Figure 13. Predicted and measured SFCC cleaning rate constant for $Re = 7{,}500$. Error bars indicate the standard deviation for three repeats.

## CONCLUSIONS

A cheap model soil based on instant coffee has been used to investigate cleaning where removal is controlled by convective mass transfer from the surface. The soil gave reproducible results and its mass diffusivity (for the components contributing to its dark colour) was determined by spinning disc and NMR diffusion techniques. These different methods gave similar estimates, of $1\times10^{-10}$ m$^2$s$^{-1}$.

Flow in the radial flow cell is laminar and is known to generate recirculation zones. These were predicted by CFD simulations and their locations corresponded to regions with noticeable changes in cleaning behaviour. Three cleaning fronts were observed in an otherwise very simple flow. The mass transport simulations predicted the observed cleaning patterns well. Flow in the duct flow is turbulent and one cleaning front is observed, which moves downstream over time. The simulations were used to estimate local cleaning fluxes for inputs to a simple calculation of the associated moving front problem. This gave reasonably good estimates of the average cleaning rate. The cleaning patterns featured streaks corresponding to locally high removal rates, reflecting striations in the turbulent flow patterns. Prediction of these features would require more detailed numerical simulations than the averaged Reynolds stress models employed here.

## Nomenclature

*Roman*

| | |
|---|---|
| $a$ | Primary cleaning front radius, m |
| $a^*$ | Scaled cleaning front location, - |
| $AR$ | Aspect ratio, - |
| $b$ | Secondary cleaning front radius, m |
| $C$ | Concentration, kg/m$^3$ |
| $C_{\mathrm{sat}}$ | Saturation concentration, kg/m$^3$ |
| $D$ | Mass diffusivity, m$^2$/s |
| $h$ | Gap height, m |
| $H$ | Head, m |
| $k'$ | Cleaning rate constant, m/s |
| $k_{\mathrm{m}}$ | Film mass transfer coefficient, m/s |
| $L$ | Characteristic length, m |
| $m_0$ | Initial soil mass coverage, kg/m$^2$ |
| $N$ | Mass flux, kg / m$^2$ s |
| $Re$ | Reynolds number, - |
| $r$ | Radial coordinate, m |
| $r_{\mathrm{in}}$ | Radius, inlet, m |
| $Sc$ | Schmidt number, - |
| $Sh$ | Sherwood number, - |
| $t$ | Time, s |
| $t_{\mathrm{c}}$ | Cleaning time, s |
| $\boldsymbol{u}$ | Velocity vector, m/s |
| $u, v$ | Velocity components, m/s |
| $x, y$ | Cartesian coordinates |

*Greek*

| | |
|---|---|
| $\delta, \delta_0$ | Soil thickness, initial value, m |
| $\rho_{\mathrm{S}}$ | Soil density, kg/m$^3$ |
| $\nu$ | Kinematic viscosity, m$^2$/s |
| $\tau_{\mathrm{w}}$ | Wall shear stress, Pa |
| $\Omega$ | Rotational speed, rad/s |



ISBN: 978-0-9984188-3-4; Published online www.heatexchanger-fouling.com

*Acronyms*

| | |
|---|---|
| CAD | Computer aided design |
| CFD | Computational fluid dynamics |
| CIP | Cleaning-in-Place |
| NMR | Nuclear magnetic resonance |
| RFC | Radial flow cell |
| RZ | Recirculation zone |
| SFCC | Slit flow cleaning cell |

**ACKNOWLEDGEMENTS**

Self-diffusion measurements were collected and analysed by Prof. M.D. Mantle. SDA data were obtained by Adolis Bagdziunas and Josh Elliott-Smith.

**REFERENCES**

[1] G. Gésan-Guiziou, A.P. Sobańtka, S. Omont, D. Froelich, M. Rabiller-Baudry, F. Thueux, D. Beudon, L. Tregret, C. Buson, D. Auffret, Life cycle assessment of a milk protein fractionation process: Contribution of the production and the cleaning stages at unit process level, *Sep. Purif. Tech.*, vol. 224, pp. 591-610, 2019.

[2] D.I. Wilson, G. Christie, P.J. Fryer, I.M. Hall, J.R. Landel and K.A. Whitehead, K.A., Lessons to learn from roadmapping in cleaning and decontamination, *Food Bioprod. Proc*., vol. 135, pp. 156–164, 2022.

[3] J. Landel and D.I. Wilson, The fluid mechanics of cleaning and decontamination of surfaces, *Ann. Rev. Fluid Mech.*, vol. 53, pp. 147-171, 2021.

[4] K.R. Goode, P.T. Robbins and P.J. Fryer, Fouling and cleaning studies in the food and beverage industry classified by cleaning type, *Comp. Reviews Food Sci. Food Safety*, vol. 12, pp. 121-143, 2013.

[5] M. Joppa, H. Köhler, F. Rüdiger, J.-P. Majschak and J. Fröhlich, Prediction of cleaning by means of computational fluid dynamics. Implication of the pre-wetting of a swellable soil, in H.U. Zettler (Ed.), *Proc*. 12th Intl Conf. Heat Exchanger Fouling & Cleaning 2017, Aranjuez, Spain, June 11-16, 2007.

[6] R.K. Bhagat, A.M. Perera and D.I. Wilson, Cleaning tank walls by moving water jets: simple models and supporting experiments, *Food Bioprod. Proc*., vol. 102, pp. 31-54, 2017.

[7] N. Gottschalk, W. Augustin, S. Scholl, D.I. Wilson and R. Mercadé-Prieto, Model soil and deposit layers for cleaning investigations, *Food Bioprod. Proc*., vol. 136, pp. 249-296, 2022.

[8] H. Köhler, V. Liebmann, C. Golla, J. Frölich, F. Rüdiger, Modeling and CFD-simulation of cleaning process for adhesively detaching film-like soils with respect to industrial application, *Food Bioprod. Proc*., Vol. 129, pp. 157-167, 2021.

[9] K.P. Deshmukh, D. Arlov, R.S. Cant, A. Göransson, F. Innings and D.I. Wilson, D.I., Cleaning of cohesive soil layers in a radial flow cell, *Food Bioprod. Proc*., vol. 136, pp. 84-9, 2022.

[10] K.P. Deshmukh, PhD Dissertation, University of Cambridge, 2024 (in preparation).

[11] M. Joppa, H.Köhler, F. Rüdiger, J.P. Majschak, J. Fröhlich, Experiments and simulations on the cleaning of a swellable soil in plane channel flow, *Heat Transf. Eng*., Vol. 38, pp. 786–795, 2017.

[12] R. Vinuesa, A. Noorani, A. Lozano-Durán, G.K.E. Khoury, P. Schlatter, P.F. Fischer, and H.M. Nagib, Aspect ratio effects in turbulent duct flows studied through direct numerical simulation, *J. Turbul*., Vol. 15, pp 677–706, 2014.

[13] G.L. Cuckston, Methods for detailed study of detergent action in cleaning food soils, PhD dissertation, University of Cambridge, 2020.

[14] R.R. Fernandes, D. Oevermann and D.I. Wilson, Cleaning insoluble viscoplastic soil layers using static and moving coherent impinging water jets, *Chem. Eng. Sci*, Vol. 207, pp. 752-768, 2019.

[15] A.A. Rashaida, D.J. Bergstrom and R.J. Sumner, Mass transfer from a rotating disk to a Bingham fluid, *J. Appl. Mech. Trans. ASME*, Vol. 73, pp. 108–111, 2006.

[16] R.Y. Nigo, Y.M.J. Chew, N.E. Houghton, W.R. Paterson and D.I. Wilson, D.I., Experimental studies of freezing fouling of model fat solutions using a novel spinning disc apparatus, *Energy & Fuels*, Vol. 23, pp. 6131–6145, 2009.

[17] K. Asteriadou, A.P.M. Hasting, M.R. Bird and J. Melrose, Predicting cleaning of equipment using computational fluid dynamics, *J. Food Proc. Eng*., Vol. 30, pp 88-105, 2007.

[18] S.I. Chernyshenko and M.F. Baig, Streaks and vortices in near-wall turbulence, *Phil. Trans. R. Soc. A*, Vol. 363, pp. 1097–1107, 2005.

[19] D.I. Wilson and A.P. Watkinson, A study of autoxidation reaction fouling in heat exchangers, *Can. J. Chem. Eng*., Vol. 74, pp. 236-246, 1996.

[20] B.P.K. Yung, H. Merry and T.R. Bott, The role of turbulent bursts in particle re-entrainment in aqueous systems, *Chem. Eng. Sci*., Vol. 44, pp. 873–882, 1988.



ISBN: 978-0-9984188-3-4; Published online www.heatexchanger-fouling.com